

# Stripe and checkerboard patterns in a stack of driven quasi-one-dimensional dipolar condensates

Shreyas Nadiger, Sandra M. Jose, Ratheejit Ghosh, Inderpreet Kaur, and Rejish Nath  
*Department of Physics, Indian Institute of Science Education and Research, Pune- 411008, India*

The emergence of transient checkerboard and stripe patterns in a stack of driven quasi-one-dimensional homogeneous dipolar condensates is studied. The parametric driving of the  $s$ -wave scattering length leads to the excitation of the lowest collective Bogoliubov mode. The character of the lowest mode depends critically on the orientation of the dipoles, corresponding to out-of-phase and in-phase density modulations in neighboring condensates, resulting in checkerboard and stripe patterns. Further, we show that a dynamical transition between the checkerboard and stripe patterns can be realized by quenching the dipole orientation either linearly or abruptly once the initial pattern is formed via periodic driving.

## I. INTRODUCTION

The long-range and anisotropic dipole-dipole interactions (DDIs) lead to many phenomena in quantum gases [1–5], including self-organized, equilibrium density patterns in Bose-Einstein condensates (BECs) [6]. The patterns also emerge when a dipolar gas is quenched or tuned to instabilities [7–12] that can be done by varying the  $s$ -wave scattering length, the number of particles, or the orientation of dipoles. Additionally, the long-range character of the DDI can lead to collective phenomena among physically disconnected condensates [13, 14]. They include dipolar drag [15, 16], hybrid excitations [17–19], soliton complexes [20–25], supersolids [26] and coupled density patterns [27]. Equilibrium checkerboard and stripe density waves are predicted to exist in disconnected dipolar gases in a planar array of one-dimensional tubes [28]. In condensates, it is found that the inter-layer interactions can significantly affect the stability criteria, even in chromium condensates for which the dipole moment is comparatively weak [29, 30]. Remarkably, a recent experiment using cold gas of dysprosium atoms demonstrates strong inter-layer dipolar effects by reducing the layer separations to 50 nm from typical lattice spacings of 500 nm [31], opening up various perspectives in the physics of dipolar gases.

When condensates are subjected to time-periodic interaction parameters [27, 32–40] or external potentials [41–49], transient density patterns are formed. For small modulation amplitudes, Bogoliubov modes of the initial state govern the periodicity of such patterns via resonant conditions [32, 43, 49]. Pattern formation under periodic driving is explored in a single [27, 33, 50, 51] and a pair of quasi-one-dimensional (Q1D) dipolar BECs [27]. However, not technically challenging, parametric driving still needs to be experimentally demonstrated in dipolar condensates. In contrast to the condensates with short-range interactions, a rotonic spectrum of a dipolar condensate can lead to unique and non-trivial wavenumber selection, making higher harmonics more unstable than lower ones [27, 33, 51]. For a pair of Q1D dipolar condensates, the long-range DDIs lead to symmetric and antisymmetric modes, which result in transient symmetric and antisymmetric Faraday patterns under periodic driving [27].

In this paper, we show that by engineering the Bogoliubov modes via dipole orientation, transient stripe, and checkerboard patterns can be created in a stack of driven Q1D homogeneous dipolar condensates. We consider the paramet-

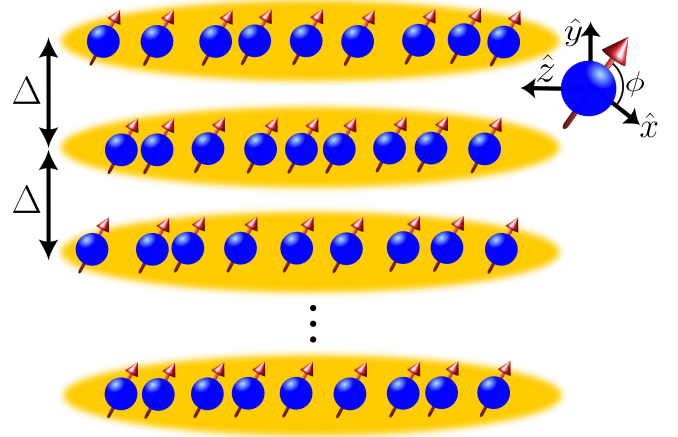


Figure 1. The schematic setup of a stack of Q1D dipolar BECs. The angle  $\phi$ , between the dipole moment and the  $x$ -axis (out of the plane), determines the nature of inter-tube DDIs, and  $\Delta$  is the separation between the adjacent Q1D condensates along the  $y$ -axis.

ric driving of the  $s$ -wave scattering length, which excites the lowest branch of the Bogoliubov spectrum. When the dipoles are aligned such that the inter-tube DDIs are repulsive, the lowest mode describes out-of-phase density modulations in neighboring condensates, leading to a checkerboard pattern. Making the inter-tube DDIs attractive, the nature of the lowest mode changes to in-phase density modulations, causing stripe patterns. Density-density correlations between the condensates in different tubes can distinguish the two patterns. Finally, we show that once the initial pattern is formed via periodic driving, quenching the dipole orientation leads to a dynamical transition between the checkerboard and stripe patterns. The differences between an abrupt quench and a linear quench are analyzed.

The paper is structured as follows. In Sec. II we introduce the setup of a stack of Q1D dipolar homogeneous BECs, the governing equations and the Bogoliubov spectrum. The Mathieu equations describing the driven condensates are discussed in Sec. III. The formation of checkerboard and stripe patterns are discussed in Secs. III A and III B, respectively. The effect of quenching of the dipole orientation on the initial pattern is analyzed in Sec. IV. Finally, we summarize and provide an

outlook in Sec. V.

## II. BEC SETUP AND BOGOLIUBOV SPECTRUM

We consider a stack of  $N$  homogeneous, Q1D dipolar BECs as shown in Fig. 1. The condensates form an array along the  $y$ -axis with a distance of  $\Delta$  between the adjacent ones.  $\Delta$  is taken sufficiently large to prevent overlap between the condensates. The dipoles are polarized in the  $xy$  plane, making an angle  $\phi$  with the  $x$ -axis. The intra-tube DDIs are repulsive irrespective of the value of  $\phi$ , whereas the inter-tube DDIs are repulsive for  $\phi = 0$  and are attractive when  $\phi = 90$  degrees. At very low temperatures, the system is described by coupled non-local Gross-Pitaevskii equations (NLGPEs),

$$i\hbar \frac{\partial \psi_j(z)}{\partial t} = \left[ -\frac{\hbar^2}{2M} \frac{\partial^2}{\partial z^2} + g n_j(z) + \frac{g_d}{3} \sum_{l=1}^N \int \frac{dq}{2\pi} e^{iqz} n_l(q) \right. \\ \left. \times F_{|l-j|}(q) \right] \psi_j(z), \quad (1)$$

where  $\psi_j(z)$  is the wave function of the  $j$ th condensate. The parameter  $g = 2\hbar^2 a_s / m l_\perp^2$  quantifies strength of short-range interactions with  $a_s$  being the s-wave scattering length and  $l_\perp = \sqrt{\hbar / m \omega_\perp}$  where  $\omega_\perp$  is the transverse trap frequency.  $g_d \propto d^2$  provides the strength of the DDIs,  $n_l(q)$  is the Fourier transform of the condensate density  $n_l(z) = |\psi_l(z)|^2$  and the function,

$$F_j(q) = \int_0^\infty dk \frac{ke^{-\frac{1}{2}k^2 l_\perp^2}}{k^2 + q^2} \left[ (k^2 - 2q^2) J_0(jk\Delta) \right. \\ \left. + 3k^2 \cos(2\phi) J_2(jk\Delta) \right], \quad (2)$$

depends on  $\phi$  and  $\Delta$ , where  $J_n(x)$  is the Bessel function of the first kind. The Q1D nature of each condensate demands  $\mu_j \ll \hbar\omega_\perp$ ,  $\forall j$  where  $\mu_j$  is the chemical potential of the  $j$ th condensate.

Considering the following solution  $\psi_j(z, t) = \left[ \sqrt{n_0} + u_j e^{i(qz - \omega t)} + v_j^* e^{-i(qz - \omega t)} \right] e^{-i\mu_j t / \hbar}$  in Eq. (1), where  $n_0$  is the homogeneous density and upto linear order in the amplitudes  $u_j$  and  $v_j$ , we obtain the coupled Bogoliubov-de Gennes equations,

$$(E_q + gn_0)u_j + gn_0 v_j + \frac{g_d n_0}{3} \sum_{l=1}^N F_{|l-j|}(q)[u_l + v_l] = \hbar\omega_j u_j \quad (3)$$

$$(E_q + gn_0)v_j^* + gn_0 u_j^* + \frac{g_d n_0}{3} \sum_{l=1}^N F_{|l-j|}(q)[u_l^* + v_l^*] = -\hbar\omega_j v_j^* \quad (4)$$

where  $E_q = \hbar^2 q^2 / 2M$ . Solving Eqs. (3) and (4), we obtain the Bogoliubov spectrum of the stack of Q1D homogeneous dipolar condensates. The long-range DDIs lead to collective modes among the condensates, with their properties depending critically on the dipole orientation (see Fig. 2). For instance, when  $\phi = 0$ , the inter-tube DDIs are repulsive, and the spectrum is dense. The lowest excitation mode has an antisymmetric character in which the density modulations in

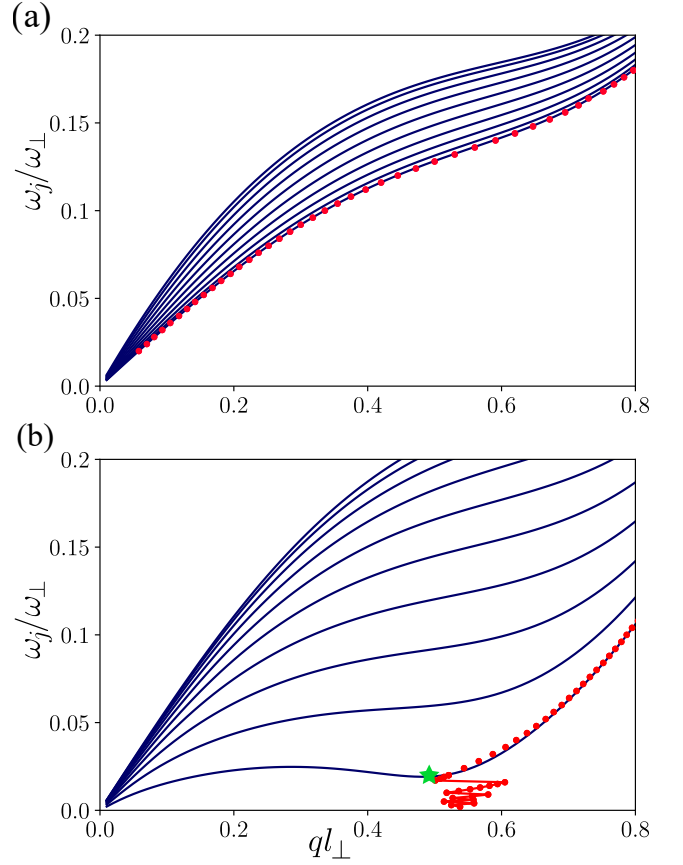


Figure 2. Bogoliubov spectrum of ten Q1D homogeneous dipolar condensates with  $gn_0 = -0.06\hbar\omega_\perp$ ,  $g_d n_0 = 0.14\hbar\omega_\perp$ , and  $\Delta = 5l_\perp$  with the dipole orientation (a)  $\phi = 0$  and (b)  $\phi = 90$  degrees. Filled circles (red) show the most unstable momentum for  $\alpha = 0.06$  as an increasing function of driving frequency  $\omega_m$ , which follows the lowest branch in (a). In contrast, as in (b), the roton minimum (marked by a star) causes a nontrivial wavenumber selection when  $\omega_m < \omega_r$ , the roton frequency of the lowest mode.

neighboring condensates are entirely out of phase. The highest excitation branch represents the in-phase density modulations between the condensates. In contrast, for  $\phi = 90$  degrees, the spectrum is sparse, and the lowest excitation branch corresponds to in-phase density oscillations due to the attractive inter-tube DDIs. The highest mode represents out-of-phase density oscillations. Thus, by tuning the dipole angle  $\phi$ , the nature of the lowest-lying mode can be engineered. We have  $g < 0$ , which results in a roton-like minimum in the lowest mode for  $\phi = 90$  degrees as shown in Fig. 2(b) [27, 33]. We restrict the interaction parameters such that the Bogoliubov spectrum is stable (purely real), and the Lee–Huang–Yang correction to the chemical potential from quantum fluctuations can be neglected [52, 53].

### III. PARAMETRIC DRIVING

In the following, we consider the parametric driving of the  $s$ -wave scattering length,  $a_s(t) = \bar{a}_s [1 + 2\alpha \cos(2\omega_m t)]$  with amplitude  $\alpha$  and frequency  $\omega_m$ . Consequently, the array of homogeneous Q1D condensates becomes unstable against forming Faraday patterns. To understand the wavenumber selection of the patterns, we introduce  $\psi_j(z, t) = \psi_j^H(z, t) [1 + K_j(t) \cos qz]$  in Eqs. (1), where

$$\psi_j^H(z, t) = \sqrt{n_0} \exp\left(-i\left[\frac{\mu_j t}{\hbar} + \frac{\alpha \bar{g} n_0}{\hbar \omega_j} \sin 2\omega_m t\right]\right)$$

is the homogeneous solution in the presence of periodic modulation with  $\bar{g} = 2\hbar^2 \bar{a}_s / m l_\perp^2$ , and  $K_j(t) = r_j(t) + i s_j(t)$  is the amplitude of the density modulation. Linearizing in  $K_j(t)$ , we arrive at the coupled equations,

$$\hbar^2 \frac{d^2 r_j}{dt^2} + E_q [E_q + 2g(t)n_0] r_j + \frac{2}{3} g_d E_q \sum_{l=1}^N F_{|l-j|}(q) r_l = 0, \quad (5)$$

which can be rewritten as

$$\hbar^2 \frac{d^2 \mathbf{R}(t)}{dt^2} + \mathcal{A} \mathbf{R}(t) = 0, \quad (6)$$

where  $\mathcal{A} = E_q [E_q + 2g(t)n_0] \mathbb{I} + \mathcal{G}(q)$ ,  $\mathbb{I}$  is an  $N \times N$  identity matrix and  $\mathbf{R} = (r_1, r_2, \dots, r_N)^T$ . The matrix  $\mathcal{G}(q)$  is given by,

$$\mathcal{G}(q) = \frac{2}{3} g_d E_q \begin{pmatrix} F_0(q) & F_1(q) & F_2(q) & \dots \\ F_1(q) & F_0(q) & F_1(q) & \dots \\ F_2(q) & F_1(q) & F_0(q) & \dots \\ \vdots & \vdots & \vdots & \ddots \end{pmatrix}, \quad (7)$$

where  $F_j(q)$  is given in Eq. (2). Equation (6) is finally decoupled into  $N$  independent Mathieu-like equations:

$$\hbar^2 \frac{d^2 \bar{r}_j}{dt^2} + [\epsilon_j^2(q) + 4\alpha \bar{g}_0 n_0 E_q \cos 2\omega_m t] \bar{r}_j = 0, \quad (8)$$

where  $\bar{r}_j = \mathbf{g}_j^T \mathbf{R}$  is the collective modulation amplitude of the stack of dipolar condensates with  $\mathbf{g}_j$  being the  $j$ th eigenvector of  $\mathcal{A}$  and  $\epsilon_j(q) = \hbar \omega_j$  is the Bogoliubov dispersion. The solutions of Eq. (8) are of the form  $\bar{r}_j(t) = f_j(t) e^{\sigma_j t}$ , where  $\sigma_j$  is the Floquet exponent and  $f_j(t) = f_j(t + 2\pi/\omega_m)$ .  $\text{Re}(\sigma_j) > 0$  indicates the dynamical instability of the stack of condensates against the formation of transient density patterns. In the limit  $\alpha \rightarrow 0$ , the unstable momenta are determined by the resonances  $n\hbar\omega_m = \epsilon_j(q)$ ,  $\forall j$ . The most unstable momentum governs the wavelength of the transient density pattern, i.e., one with the largest  $\text{Re}(\sigma_j)$ . It is further verified by numerically solving the coupled NLGPEs (1) starting from a homogeneous solution with a tiny random noise embedded in it.

#### A. Checkerboard pattern

First, we consider dipoles oriented along the  $x$ -axis ( $\phi = 0$ ). In this case, the inter-tube DDIs along the  $y$ -axis are repulsive,

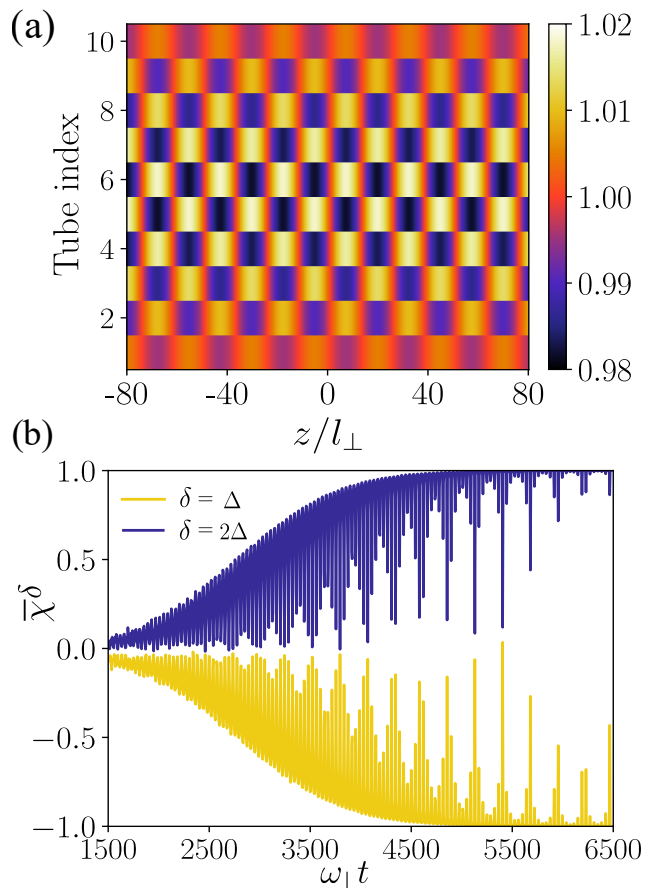


Figure 3. (a) Checkerboard density pattern and (b) the corresponding density-density correlations in a stack of ten Q1D dipolar condensates for  $\phi = 0$ ,  $g n_0 = -0.06\hbar\omega_\perp$ ,  $g_d n_0 = 0.14\hbar\omega_\perp$ ,  $\Delta = 5l_\perp$ ,  $\alpha = 0.06$  and  $\omega_m = 0.08\omega_\perp$ . The snapshot of the pattern is taken at  $\omega_\perp t = 6500$ . While plotting, we have taken a finite width of the condensate along the transverse  $y$ -direction for better visualization. The average density-density correlation  $\bar{\chi}^\delta$  is obtained for nearest ( $\delta = \Delta$ ) and next-nearest condensates ( $\delta = 2\Delta$ ).

and the lowest mode in the Bogoliubov spectrum characterizes out-of-phase density modulations in neighboring condensates. Upon periodic driving, the solutions of the Eq. (8) reveal that the dominant unstable momenta are provided by the resonances  $\hbar\omega_m = \epsilon_j(q)$ , which are  $N$  in the count for a given driving frequency. Since the Floquet exponent  $\sigma_j(q)$  is proportional to  $q^2$  [33], the highest among the  $N$  momenta, which is that of the lowest mode, is the most unstable [see Fig. 2(a)]. The excitation of the lowest mode leads to a checkerboard density pattern, as shown in Fig. 3(a), where the numerical results are shown for ten Q1D condensates. Due to the finite number of tubes, the lowest mode has a larger amplitude for the central condensate, decreasing as we move to the outer ones. As a consequence, the contrast of the pattern is also minimal in the outer condensates.

Further, to characterize the pattern, we calculate the density-density correlation function between a pair of conden-

sates,

$$\chi^{(j,k)}(t) = \int dz \frac{S_j(z,t)S_k(z,t)}{\sqrt{(\int dz S_j^2(z,t))(\int dz S_k^2(z,t))}} \quad (9)$$

where  $S_j(z,t) = n_j(z,t) - n_0$  with  $j$  denoting the tube index along the  $y$ -axis. The average density-density correlation among all pairs of tubes separated by a distance  $\delta$  is defined as,

$$\bar{\chi}^\delta(t) = \frac{1}{N - \delta/\Delta} \sum_{j=1}^{N-\delta/\Delta} \chi^{(j,j+\delta/\Delta)}(t). \quad (10)$$

In Fig. 3(b), we show  $\bar{\chi}^\delta(t)$  of the checkerboard pattern for neighbouring ( $\delta = \Delta$ ) and nearest-neighbouring ( $\delta = 2\Delta$ ) condensates. Between the neighboring condensates, the density modulations are out of phase, making  $\bar{\chi}^{\delta=\Delta}(t) < 0$ . Since the amplitude of the density pattern oscillates with the driving frequency,  $\bar{\chi}^\delta(t)$  also exhibits oscillations of frequency  $\omega_m$ . Eventually,  $\bar{\chi}^{\delta=\Delta}(t)$  attains a minimum value of  $\sim -1$ , indicating a maximally anticorrelated density pattern between neighboring condensates. In contrast, the density modulations are in phase between next-nearest-neighbor condensates, leading to a maximal value of  $\sim +1$  for  $\bar{\chi}^{\delta=2\Delta}(t)$  at longer times. It means condensates separated by odd multiples of  $\Delta$  are anti-correlated, and even multiples are correlated.

### B. Stripe pattern

Changing the dipole orientation from  $x$ -axis ( $\phi = 0$ ) to  $y$ -axis ( $\phi = 90$  degrees) changes the lowest mode character from out-of-phase to in-phase density modulations between the neighboring condensates. It leads to the formation of a stripe pattern when the  $s$ -wave scattering length is modulated [see Fig. 4(a)]. For the stripe pattern,  $\bar{\chi}^\delta$  is positive irrespective of  $\delta$ . At longer times,  $\bar{\chi}^\delta \sim 1$  indicates a fully correlated stripe pattern [see Fig. 4(b)]. The larger the  $\delta$ ,  $\bar{\chi}^\delta$  takes more time to saturate to unity. Even though the most unstable momentum follows the lowest branch in Fig. 2(b), the presence of a roton minimum puts an upper cutoff to the pattern wavelength  $\sim 1/q_r$  since the higher harmonics having energy closer to the roton minimum become more unstable at low driving frequencies [27, 33, 51].

## IV. QUENCHING THE DIPOLE ORIENTATION: DYNAMICAL PATTERN TRANSITIONS

Interestingly, once the pattern is formed via periodic driving, quenching the dipole orientation or the angle  $\phi$  leads to the dynamical transition between the checkerboard and stripe patterns. For instance, when  $\phi = 0$  initially, the periodic driving leads to a checkerboard pattern. After the amplitude of the checkerboard pattern reaches sufficiently high, the periodic driving is stopped and simultaneously quenches  $\phi$  to 90 degrees. The latter causes a transition dynamically from

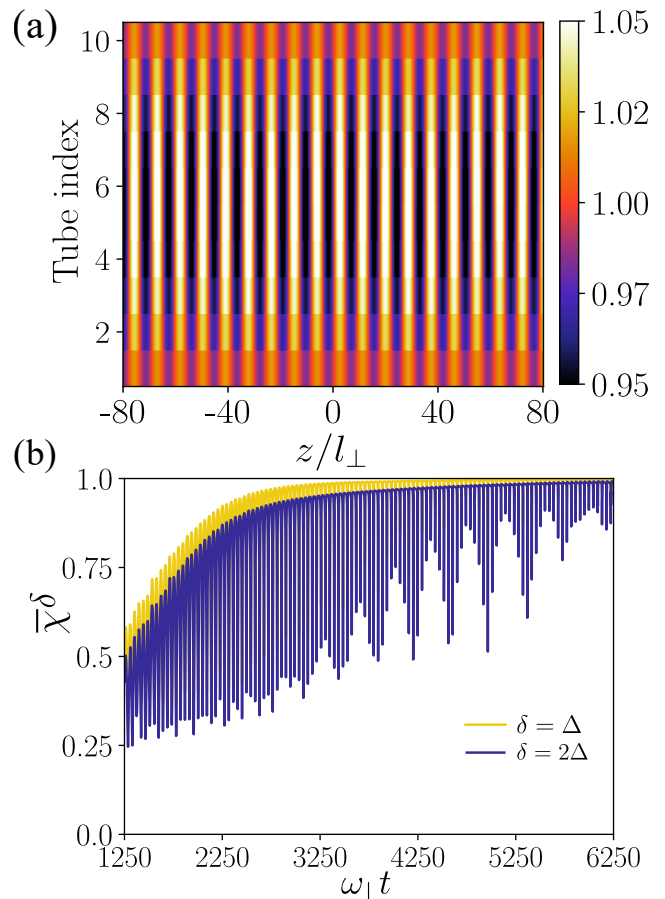


Figure 4. (a) Stripe density pattern and (b) the corresponding density-density correlations in a stack of ten Q1D dipolar condensates for  $\phi = 90$  degrees,  $gn_0 = -0.06\hbar\omega_\perp$ ,  $g_{an_0} = 0.14\hbar\omega_\perp$ ,  $\Delta = 5l_\perp$ ,  $\alpha = 0.01$  and  $\omega_m = 0.07\omega_\perp$ . The snapshot of the pattern is taken at  $\omega_\perp t = 6185$ . The average density-density correlation  $\bar{\chi}^\delta$  is shown for nearest ( $\delta = \Delta$ ) and next-nearest condensates ( $\delta = 2\Delta$ ). While plotting, we have taken a finite width of the condensate along the transverse  $y$ -direction for better visualization.

the checkerboard pattern to a stripe pattern. Similarly, starting from  $\phi = 90$  degrees, creating a stripe pattern, and then quenching  $\phi$  to zero leads to stripe to checkerboard transition. Below, we compare two cases of quenching: instantaneous and linear.

### A. Instantaneous quench

The first row of Fig. 5 shows the dynamical transition of patterns due to the instantaneous quench of  $\phi$  from zero to 90 degrees. First, we form the checkerboard pattern for  $\phi = 0$  via periodic modulation [see Fig. 5(a)]. Then, the driving is stopped and instantly quenches  $\phi$  to 90 degrees. The quenching distorts the checkerboard pattern since the inter-tube DDIs (along the  $y$ -axis) abruptly changed from maximally repulsive ( $\phi = 0$ ) to maximally attractive ( $\phi = 90$  degrees). In particular, each density peak in the checkerboard pattern breaks

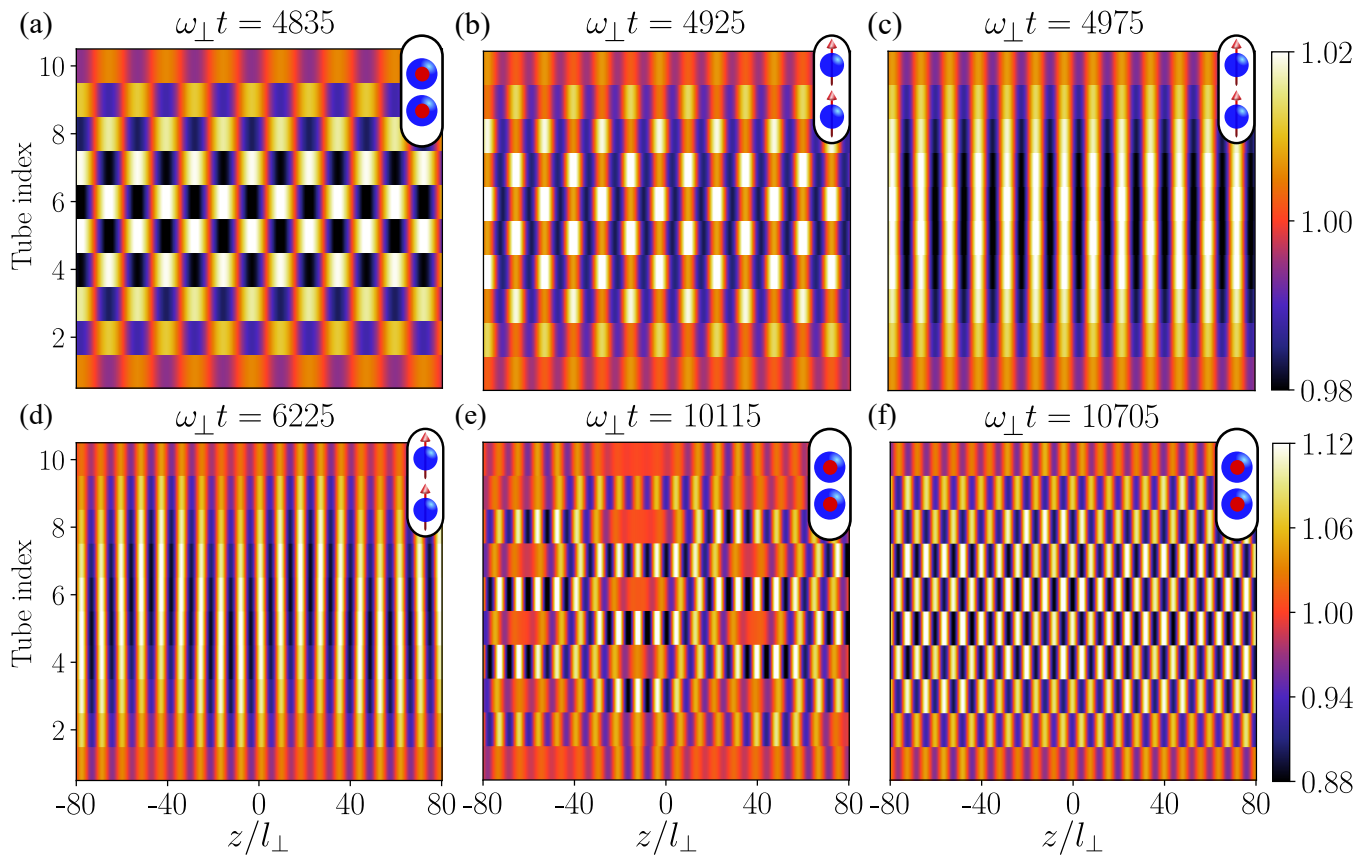


Figure 5. Dynamical pattern transition under instantaneous quench of dipole orientation. (a)-(c) shows the pattern transition when  $\phi$  is quenched from zero to 90 degrees, and (d)-(f) shows the same for the reverse case. The instant of time for each density snapshot is provided at the top of each figure. For (a)-(c), the modulation parameters are  $\omega_m = 0.08\omega_\perp$  and  $\alpha = 0.08$ . The dipole angle  $\phi$  is quenched at  $\omega_\perp t = 4850$ . For (d)-(f),  $\omega_m = 0.07\omega_\perp$  and  $\alpha = 0.01$  and we quench at  $\omega_\perp t = 6250$ . The orientation of the dipoles is shown in each figure. The other parameters are  $gn_0 = -0.06\hbar\omega_\perp$ ,  $g_d n_0 = 0.14\hbar\omega_\perp$ , and  $\Delta = 5l_\perp$ .

into two due to the attractive pull from the density peaks on either side of the neighboring tubes. Eventually, they align into stripe patterns as shown in Figs. 5(b) and 5(c). The intermediate stripe pattern in Fig. 5(b) also exhibits a density modulation along each stripe. The breaking of density peaks makes the spatial periodicity of the stripe pattern half that of the initial checkerboard pattern. Similarly, in the second row of Fig. 5, the pattern transition due to the quenching  $\phi$  from 90 degrees to zero is shown. The initial stripe pattern dynamically changes to a checkerboard pattern after the sudden quench of  $\phi$  as shown in Figs. 5(d)-5(f).

The evolution of the correlation  $\bar{\chi}^\delta$  during the pattern transition is shown in Fig. 6. In Fig. 6(a), the nearest neighbor correlation ( $\delta = \Delta$ ) changes from negative to positive, whereas the next nearest neighbor ( $\delta = 2\Delta$ ) remains positive, indicating the transition from a checkerboard to a stripe pattern. In contrast, for the stripe to checkerboard transition,  $\bar{\chi}^{\delta=\Delta}$  changes its sign from positive to negative [see Fig. 6(b)]. For a fixed  $g$  and  $g_d$ , the maximally attractive ( $\phi = 90$  degrees) inter-tube DDI is two times stronger than the maximally repulsive ( $\phi = 0$ ) one, causing the checkerboard to stripe transition much quicker than the stripe to checkerboard transition.

In general, the transition period between the patterns depends on several factors, particularly the pattern amplitude before the quenching. The longer the initial periodic driving, (before the condensates get destroyed by heating) the larger the amplitude and the stronger the DDIs between the density peaks in the neighboring tubes. The latter can augment the speed of the pattern transition upon the abrupt quench. At the same time, periodic driving also increases the average kinetic energy. The quenching further excites the vibrational modes of the initial transient crystalline-like pattern, which can lead to subsequent dynamical oscillations between the two patterns, as evident in the dynamics of the density correlations.

## B. Linear quench

The linear quench also results in similar dynamics to the abrupt quench. The main difference is that the transition period has been prolonged. In particular, that of stripe to checkerboard transition since inter-tube DDIs change gradually from attractive to repulsive, but the repulsive strength is weaker than the attractive counterpart. The delay in transition



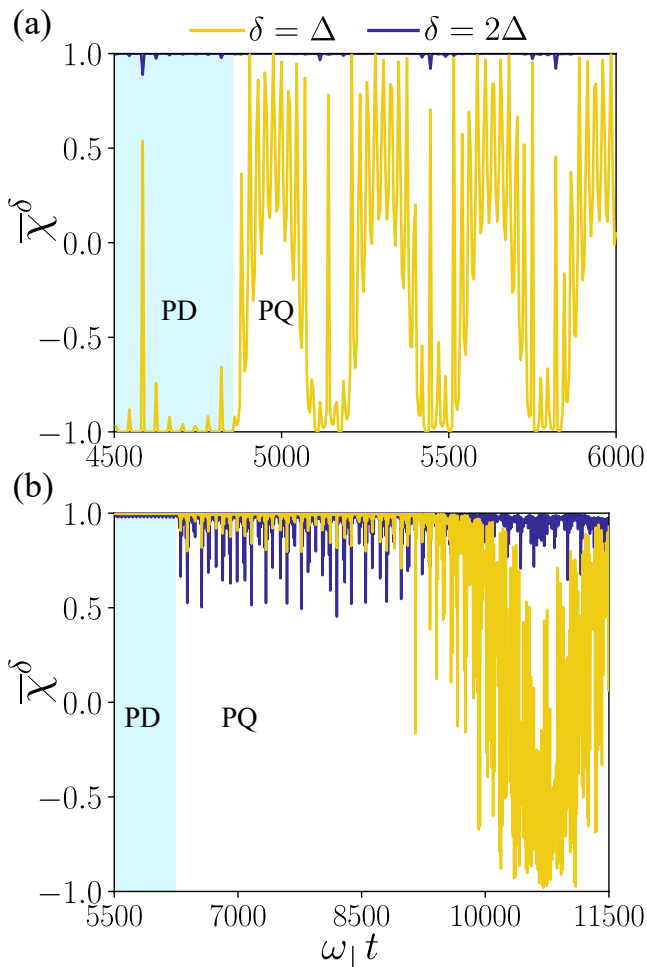


Figure 6. *Abrupt quench.* The evolution of density-density correlation function  $\bar{\chi}^\delta$  for the driven-quench dynamics with (a)  $\phi = 0$  to  $\phi = 90$  degrees and (b)  $\phi = 90$  degree to  $\phi = 0$  quenches. For (a), the modulation parameters are  $\omega_m = 0.08\omega_\perp$  and  $\alpha = 0.08$  and for (b),  $\omega = 0.07\omega_\perp$  and  $\alpha = 0.01$ . The other parameters are the same as in Fig. 5. In (a) the quench is done at  $\omega_\perp t = 4850$  and in (b) at  $\omega_\perp t = 6250$ . PD stands for periodic driving, and PQ stands for post-quench.

is also evident in the dynamics of the density-density correlations shown in Fig. 7. A new scenario that can emerge is that a linear quench may not significantly excite the vibrational modes of the transient crystalline pattern. Hence, a complete revival of the initial pattern may not occur after the transition.

## V. SUMMARY AND OUTLOOK

Summarizing, we analyzed the formation of checkerboard and stripe patterns in a stack of driven Q1D homogeneous dipolar condensates. The parametric driving of  $s$ -wave scattering length excited the lowest Bogoliubov mode. The checkerboard and stripe patterns are observed by engineering the lowest mode via the dipole orientation. The dynamical transition between the two patterns is seen by either abruptly

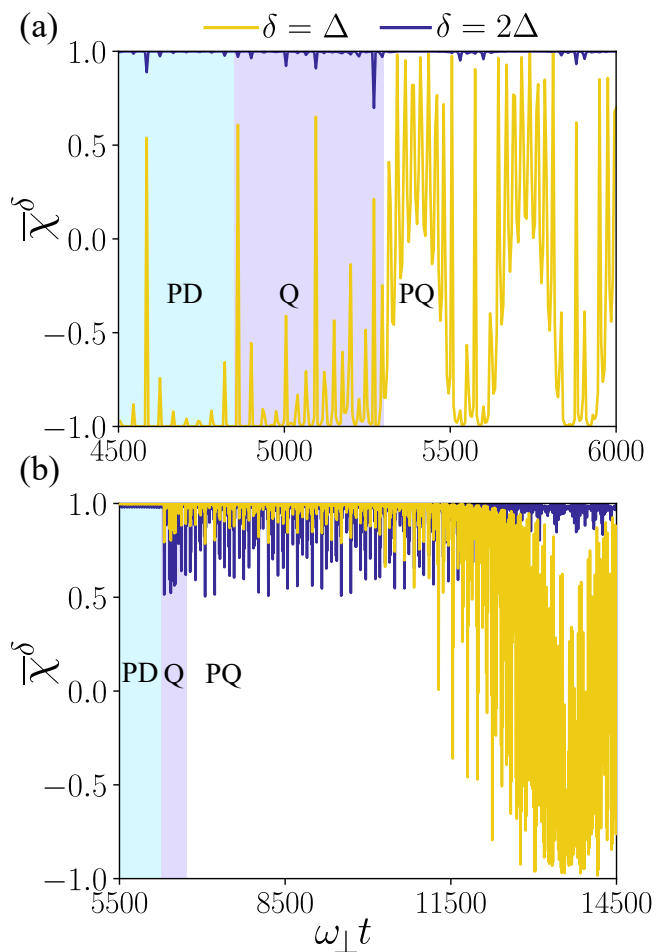


Figure 7. *Linear quench.* The evolution of density-density correlation function  $\bar{\chi}^\delta$  for the driven-quench dynamics with (a)  $\phi = 0$  to  $\phi = 90$  degrees and (b)  $\phi = 90$  degree to  $\phi = 0$  quenches. For (a), the modulation parameters are  $\omega_m = 0.08\omega_\perp$  and  $\alpha = 0.08$  and for (b),  $\omega = 0.07\omega_\perp$  and  $\alpha = 0.01$ . The other parameters are the same as in Fig. 5. In (a) the quench is started at  $\omega_\perp t = 4850$  and ends at  $\omega_\perp t = 5295$ , and in (b) from  $\omega_\perp t = 6250$  to  $\omega_\perp t = 6695$ . PD stands for periodic driving, Q for the regime of quench and PQ for post-quench.

or linearly quenching the dipole orientation after the initial pattern is formed via parametric driving.

Our studies open up several exciting perspectives. One aspect would be designing driving schemes to selectively excite any mode in the Bogoliubov spectrum of a stack of disconnected dipolar condensates. Second, to investigate the nature of patterns at an arbitrary orientation of the dipoles and their response to quenching of different interaction parameters. The studies can also easily extend two-dimensional multi-layer dipolar BECs, where the coupled patterns can be more complex.

## VI. ACKNOWLEDGEMENTS

We acknowledge National Supercomputing Mission (NSM) for providing computing resources of "PARAM Brahma" at IISER Pune, which is implemented by C-DAC

and supported by the Ministry of Electronics and Information Technology (MeitY) and Department of Science and Technology (DST), Government of India. R.N. further acknowledges DST-SERB for Swarnajayanti fellowship File No. SB/SJF/2020-21/19, and the MATRICS grant (MTR/2022/000454) from SERB, Government of India. S.N. acknowledges funding from DST through KVPY scholarship.

- 
- [1] M. A. Baranov, *Physics Reports* **464**, 71 (2008).
- [2] T. Lahaye, C. Menotti, L. Santos, M. Lewenstein, and T. Pfau, *Reports on Progress in Physics* **72**, 126401 (2009).
- [3] M. A. Baranov, M. Dalmonte, G. Pupillo, and P. Zoller, *Chemical Reviews* **112**, 5012 (2012).
- [4] L. Chomaz, I. Ferrier-Barbut, F. Ferlaino, B. Laburthe-Tolra, B. L. Lev, and T. Pfau, *Reports on Progress in Physics* **86**, 026401 (2023).
- [5] N. Defenu, T. Donner, T. Macrì, G. Pagano, S. Ruffo, and A. Trombettoni, *Rev. Mod. Phys.* **95**, 035002 (2023).
- [6] J. Hertkorn, J.-N. Schmidt, M. Guo, F. Böttcher, K. S. H. Ng, S. D. Graham, P. Uerlings, T. Langen, M. Zwierlein, and T. Pfau, *Phys. Rev. Res.* **3**, 033125 (2021).
- [7] R. Nath, P. Pedri, and L. Santos, *Phys. Rev. Lett.* **102**, 050401 (2009).
- [8] A. Macia, D. Hufnagl, F. Mazzanti, J. Boronat, and R. E. Zillich, *Phys. Rev. Lett.* **109**, 235307 (2012).
- [9] M. Raghunandan, C. Mishra, K. Łakomy, P. Pedri, L. Santos, and R. Nath, *Phys. Rev. A* **92**, 013637 (2015).
- [10] C. Mishra and R. Nath, *Phys. Rev. A* **94**, 033633 (2016).
- [11] K.-T. Xi, T. Byrnes, and H. Saito, *Phys. Rev. A* **97**, 023625 (2018).
- [12] H. Zhang, S. Liu, and Y.-S. Zhang, *Phys. Rev. A* **105**, 063319 (2022).
- [13] A. Junginger, J. Main, and G. Wunner, *Phys. Rev. A* **82**, 023602 (2010).
- [14] M. Rosenkranz, Y. Cai, and W. Bao, *Phys. Rev. A* **88**, 013616 (2013).
- [15] N. Matveeva, A. Recati, and S. Stringari, *The European Physical Journal D* **65**, 219 (2011).
- [16] A. Gallemi, M. Guilleumas, R. Mayol, and M. Pi, *Journal of Physics: Conference Series* **497**, 012035 (2014).
- [17] M. Klawunn and L. Santos, *Phys. Rev. A* **80**, 013611 (2009).
- [18] C.-C. Huang and W.-C. Wu, *Phys. Rev. A* **82**, 053612 (2010).
- [19] A. Maluckov, G. Gligorić, L. c. v. Hadžievski, B. A. Malomed, and T. Pfau, *Phys. Rev. A* **87**, 023623 (2013).
- [20] R. Nath, P. Pedri, and L. Santos, *Phys. Rev. A* **76**, 013606 (2007).
- [21] P. Köberle and G. Wunner, *Phys. Rev. A* **80**, 063601 (2009).
- [22] K. Łakomy, R. Nath, and L. Santos, *Phys. Rev. A* **86**, 013610 (2012).
- [23] K. Łakomy, R. Nath, and L. Santos, *Phys. Rev. A* **85**, 033618 (2012).
- [24] K. M. Elhadj, A. Boudjemâa, and U. Al-Khawaja, *Physica Scripta* **94**, 085402 (2019).
- [25] G. Hegde, P. Nayak, R. Ghosh, and R. Nath, *J. Phys. B: At., Mol. Opt. Phys.* **54**, 205301 (2021).
- [26] P. Nayak, R. Ghosh, and R. Nath, "Density engineering via inter-condensate dipole-dipole interactions: axial confinement and supersolids," (2023), [arXiv:2309.13000 \[cond-mat.quant-gas\]](https://arxiv.org/abs/2309.13000).
- [27] K. Łakomy, R. Nath, and L. Santos, *Phys. Rev. A* **86**, 023620 (2012).
- [28] C. Kollath, J. S. Meyer, and T. Giamarchi, *Phys. Rev. Lett.* **100**, 130403 (2008).
- [29] S. Müller, J. Billy, E. A. L. Henn, H. Kadau, A. Griesmaier, M. Jona-Lasinio, L. Santos, and T. Pfau, *Phys. Rev. A* **84**, 053601 (2011).
- [30] R. M. Wilson and J. L. Bohn, *Phys. Rev. A* **83**, 023623 (2011).
- [31] L. Du, P. Barral, M. Cantara, J. de Hond, Y.-K. Lu, and W. Ketterle, "Atomic physics on a 50 nm scale: Realization of a bilayer system of dipolar atoms," (2023), [arXiv:2302.07209 \[cond-mat.quant-gas\]](https://arxiv.org/abs/2302.07209).
- [32] K. Staliunas, S. Longhi, and G. J. de Valcárcel, *Phys. Rev. Lett.* **89**, 210406 (2002).
- [33] R. Nath and L. Santos, *Phys. Rev. A* **81**, 033626 (2010).
- [34] N. Katz and O. Agam, *New J. Phys.* **12**, 073020 (2010).
- [35] J. H. V. Nguyen, M. C. Tsatsos, D. Luo, A. U. J. Lode, G. D. Telles, V. S. Bagnato, and R. G. Hulet, *Phys. Rev. X* **9**, 011052 (2019).
- [36] Z. Zhang, K.-X. Yao, L. Feng, J. Hu, and C. Chin, *Nat. Phys.* **16**, 652 (2020).
- [37] K. Kwon, K. Mukherjee, S. J. Huh, K. Kim, S. I. Mistakidis, D. K. Maity, P. G. Kevrekidis, S. Majumder, P. Schmelcher, and J.-y. Choi, *Phys. Rev. Lett.* **127**, 113001 (2021).
- [38] S. M. Jose, K. Sah, and R. Nath, *Phys. Rev. A* **108**, 023308 (2023).
- [39] K. Fujii, S. L. Görlitz, N. Liebster, M. Sparn, E. Kath, H. Strobel, M. K. Oberthaler, and T. Enss, "Square pattern formation as stable fixed point in driven two-dimensional bose-einstein condensates," (2023), [arXiv:2309.03829 \[cond-mat.quant-gas\]](https://arxiv.org/abs/2309.03829).
- [40] N. Liebster, M. Sparn, E. Kath, K. Fujii, S. Görlitz, T. Enss, H. Strobel, and M. K. Oberthaler, "Emergence of crystalline steady state in a driven superfluid," (2023), [arXiv:2309.03792 \[cond-mat.quant-gas\]](https://arxiv.org/abs/2309.03792).
- [41] K. Staliunas, S. Longhi, and G. J. de Valcárcel, *Phys. Rev. A* **70**, 011601 (2004).
- [42] M. Modugno, C. Tozzo, and F. Dalfovo, *Phys. Rev. A* **74**, 061601 (2006).
- [43] P. Engels, C. Atherton, and M. A. Hofer, *Phys. Rev. Lett.* **98**, 095301 (2007).
- [44] A. I. Nicolin, R. Carretero-González, and P. G. Kevrekidis, *Phys. Rev. A* **76**, 063609 (2007).
- [45] A. I. Nicolin, *Phys. Rev. E* **84**, 056202 (2011).
- [46] A. Balaž and A. I. Nicolin, *Phys. Rev. A* **85**, 023613 (2012).
- [47] A. Balaž, R. Paun, A. I. Nicolin, S. Balasubramanian, and R. Ramaswamy, *Phys. Rev. A* **89**, 023609 (2014).
- [48] G. Verma, U. D. Rapol, and R. Nath, *Phys. Rev. A* **95**, 043618 (2017).
- [49] R. Cominotti, A. Berti, A. Farolfi, A. Zenesini, G. Lamporesi, I. Carusotto, A. Recati, and G. Ferrari, *Phys. Rev. Lett.* **128**, 210401 (2022).

- [50] D. Vudragović and A. Balaž, *Symmetry* **11** (2019), [10.3390/sym11091090](https://doi.org/10.3390/sym11091090).
- [51] B. K. Turmanov, B. B. Baizakov, and F. K. Abdullaev, *Phys. Rev. A* **101**, 053616 (2020).
- [52] D. Edler, C. Mishra, F. Wächtler, R. Nath, S. Sinha, and L. Santos, *Phys. Rev. Lett.* **119**, 050403 (2017).
- [53] A. Pricoupenko and D. S. Petrov, *Phys. Rev. A* **103**, 033326 (2021).